Nonimaging Beam Combiner-Collimator

Contract No. DAAD17-99-C-0024

Competitively Awarded

Contract Amount: $119,967

Final Report

Presented to:
U.S. Army Research Laboratory

Technical Monitor:
Mr. Barry Stann/AMSRL-SE-EE
U.S. Army Research Laboratory
2800 Powder Mill Road
Adelphi, MD 20783-1197

Presented by:
Physical Optics Corporation
Applied Technology Division
2545 W. 237th Street, Suite B
Torrance, California 90505
(310) 530-1416
CAGE NO. OAZ36

Principal Investigator:
Ilya Agurok, Ph.D.

November 1999

Distribution Statement A: Approved for public release; distribution is unlimited.

ABSTRACT

In this Phase I SBIR project, Physical Optics Corporation (POC) experimentally demonstrated an innovative concept of a nonimaging beam combiner-concentrator (NIBCC). POC designed and fabricated the NIBCC prototype, which consists of three laser diodes coupled to optical fibers, three GRIN lens objectives for focusing light into the NIBCC focal point, a mechanical assembly for aligning the focusing device, and the beam combiner. The designed divergence of the outgoing beam is ±3 minutes, which provides a 10 m light spot at a 5 km distance. In the NIBCC prototype, we achieved ±5.5 minutes divergence. The excess divergence in the NIBCC prototype is due to several factors that will be eliminated during Phase II. The prototype built during Phase I proved the potential of the proposed device and created a foundation for its further development to achieve the required characteristics.

1.0 INTRODUCTION

The Army Research Laboratory (ARL) is investigating low-cost imaging laser radar technologies for battlefield applications [1] as part of the Multi-Domain Smart Sensor (MDSS) systems currently under development by the ARL [2]. The Army Service and Technology Board considers the MDSS a high-payoff technology for the Army because imaging radar can concurrently obtain the distance to each pixel in an illuminated spot and is consequently very effective at recognizing camouflaged objects by making a 3-D rendering of the battle scene from different points of view. Thus targets and cluttered environments can effectively be separated. To obtain high fidelity 3-D images in a sufficient signal-to-noise ratio environment, laser power of ~20 W is required. For a multi-object scene, the high output power provided by radar is necessary. At the present time, the highest power laser diodes can produce no more than 1 to 4 Watts. Therefore, the ARL is searching for an effective way to combine the power from up to 20 lasers in one beam with a low 2 mrad (6 arc minutes) divergence to provide an illumination of objects as large as 10 meters at a distance of up to 5 km. To support ARL's radar development [1], it is necessary to create a beam combiner that is phase coherent at microwave modulation frequencies of~1 GHz. Thus, in response to the ARL solicitation, POC proposed a nonimaging beam combiner [3].

1.1 POC's Solution

POC combined two recently developed advanced technologies: a nonimaging optics approach for the collimating optics [4,5] and a gradient index (GRIN) lens technology [6] for focusing outgoing light from the fibers at the focal point of a nonimaging element (NIE). The proposed nonimaging beam combiner-collimator (NIBCC) system is shown in Figure 1-1.

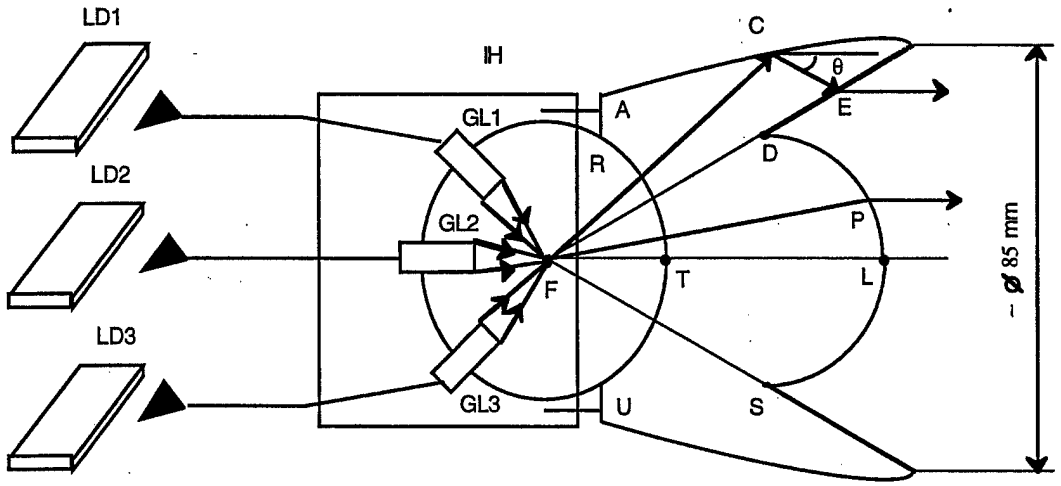

Figure 1-1
Nonimaging beam combiner-collimator (NIBCC): NIE = nonimaging element; IH = illumination housing.

As seen in Figure 1-1, the light from a number of laser diodes (LD_1, LD_2, LD_3) is coupled to the fibers, using either horn technology [7] or conventional optics [8]. A number of GRIN lenses ($GL_{1,2,3}$) steer light to the focal point F of the NIE. Each array of GRIN lenses is placed in an illuminator housing (IH) that is centered on the NIE.

The original NIE consists of surfaces with rotation symmetry [5]. As the schematic in Figure 1-1 shows, the RTU entrance surface is spherical, with its center at point F. The rays from point F go through this surface without refraction. Surface AB includes a parabola with its focus at point F. Every ray FC will be reflected (as ray CE) in a direction parallel to the parabola's axis through total internal reflection [9]. The conical surface BD will refract ray CE in a direction parallel to the NIE axis. The surface DLS is ellipsoid, with the back focus at point F. This surface will directly refract incident rays (FP in Figure 1-1) in a direction parallel to the NIE axis [9]. The acquisition angle of this NIE is 180° (i.e., the NIE can collect light from a π solid angle). It is also an aberration-free collimating element for point sources. Because the focusing spot size at point F can be extremely small (~50 μm), this NIE will provide 0.5 mrad divergence of the outgoing beam. To support low aberrations in the NIE (made from optical plastic, using diamond turning technology), the acquisition angle must be reduced to 160°. This reduction in the acquisition angle does not significantly reduce the amount of collected light.

The proposed nonimaging beam combiner-collimator offers the following advantages:

- It achieves a high quality collimated beam with 0.5 mrad divergence.
- It is mechanically rugged and doesn't require periodical alignment during the operational period, even under battlefield conditions.
- It can be inexpensively mass produced by either molding or diamond-turning technologies.
- It is transparent to enemy radar because it can be made without metal elements; therefore, it supports stealth technology.
- It is very compact, 10 times smaller than a conventional optics approach; we expect the size of the NIBCC to be $< 2" \times 2" \times 3"$.
- It is stable against contamination, with an outer surface that can be easily cleaned.
- It provides phase coherent collimation at microwave modulation frequencies of 1 GHz, because the optical path difference in the NIBCC can be designed to be much less than the coherence length of a 1 GHz microwave signal.
- It provides high-efficiency (>98%, with antireflection coating on the NIBCC) light collimation.
- The more beams the NIBCC has to combine, the smaller every partial aperture of the entrance beam; hence, potential aberrations of individual beams are also smaller.
- The proposed NIBCC can combine beams of the same wavelength. All the devices based on the property of diffraction gratings can combine beams with slightly different wavelengths into one beam. This will prevent combining a large number of beams.

The proposed NIBCC is very inexpensive and maintains its stability in the presence of temperature deviations and vibrations. Because of its ability to achieve high brightness in small, solid angles, it will be attractive in many commercial applications such as airport landing lights, warning approach lights for high masts, police searchlights, and helicopter approach lights.

1.2 Principles of Nonimaging Beam Combiner Design

1.1.2 Imaging and Nonimaging Approach in the Design of Optical Beam Transformers

There are two main approaches in optics for transforming light: flux-imaging and nonimaging. In imaging optics, there is an unambiguous correspondence between the points of the object and the image. This correspondence is shown in Figure 1-2 for a projection lens.

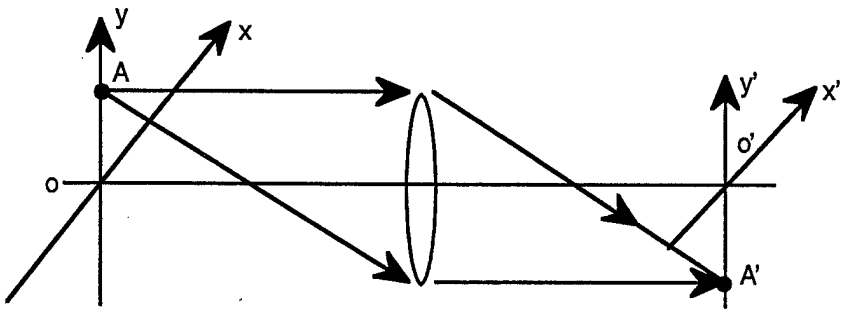

Figure 1-2
Correspondence between object and image.

Although the correspondence between points A and A' can be distorted by small aberrations, we still can consider point A' to be an image of point A. The coordinates of the object points and the image points in Figure 1-2 are Cartesian coordinates in coordinate systems (x, y) and (x', y'). For an object at infinity or at a very large distance (as in astronomical telescopes), the coordinates of the object points are the direct cosines of the incident beams that originate from the remote object points.

A conical light concentrator is a classic example of nonimaging optics, as shown in Figure 1-3.

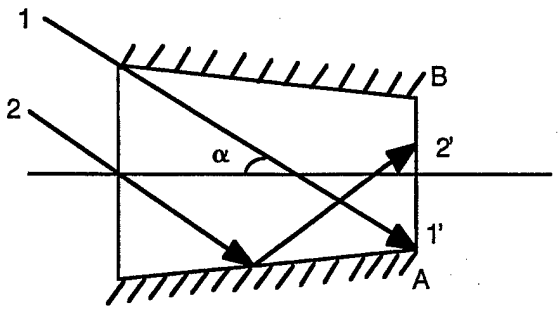

Figure 1-3
Conical light concentrator.

This light concentrator collects light from a remote light source to the absorber at the end of the concentrator segment AB. The light of beams incident at angles between $\pm\alpha$ is collected. For two rays with an incident angle α, ray 1 and ray 2, from one point of a remote object, image points 1' and 2' are located at significantly different places. The important feature of a nonimaging element is the existence of several paths for rays that originate from one object point. This is shown in Figure 1-3. Ray 1 goes directly to the image, but ray 2 is reflected from a conical surface. Because of these two attributes, the proposed beam combiner can be considered a nonimaging element, as shown in Figure 1-4.

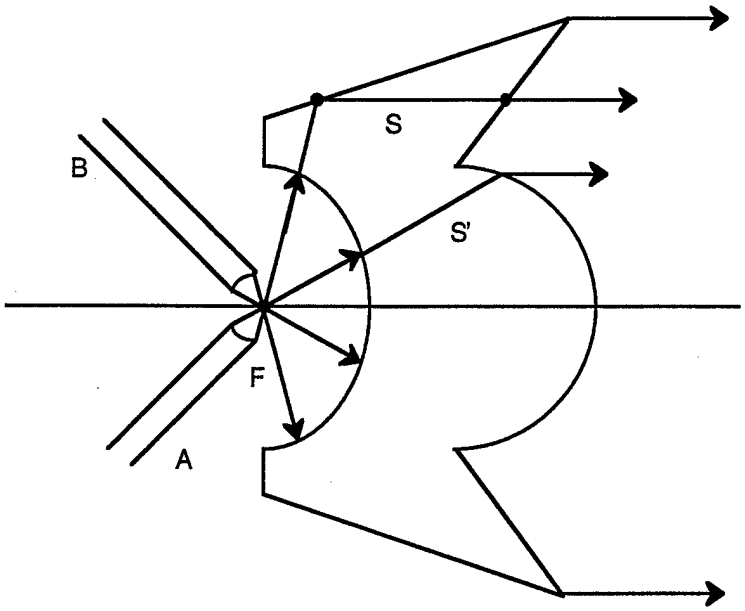

Figure 1-4
POC's beam combiner.

The two objects A and B are imaged into one outgoing collimated beam. There are two paths through the beam combiner for every ray bundle. These are optical paths S and S' in Figure 1-4.

1.2.2 Existing Nonimaging Collimator Technique

Nonimaging, reflective, incident-light concentrators that increase the efficiency of photodetection have been studied intensively over the last two decades [4,12-13]. A compound parabolic concentrator (CPC) [4] is a typical example of these kinds of devices. It can collect light into a flat fiber bundle area or collimate light from the bundle (see Figure 1-5).

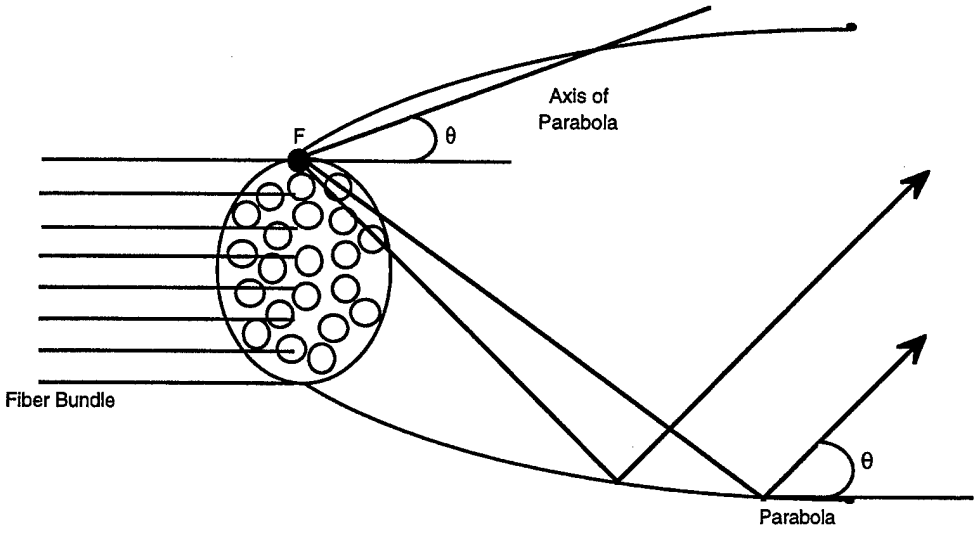

Figure 1-5
Compound parabolic concentrator.

The CPC collimates the beam perfectly from the edge of the fiber bundle at point F, which is the focus of the inclined parabola. The axis of the parabola is at an angle θ to the CPC axis, so that all the edges of the flat bundle are perfectly collimated in a conical beam with an angle θ with respect to the CPC axis. This is the edge-ray principle of nonimaging collimator design [4]. This principle assumes that all light from points inside the bundle will be collimated inside a cone of ±θ. This assertion is based on the very general consideration of an optical system as a system

that achieves topological, continuous mapping of the object area to the image area. According to the fundamental topological theory of continuous mapping, if the borders of object area are mapped into the border of the image area, the inside object points will be mapped inside the image area. The three-dimensional consideration demonstrates significant imperfection. Usually, we can concentrate the light from a flat fiber bundle end into a cone of several degrees, with a CPC length of about 300 mm.

Typical transmission curves that can be achieved by using the CPC design are shown in Figure 1-6.

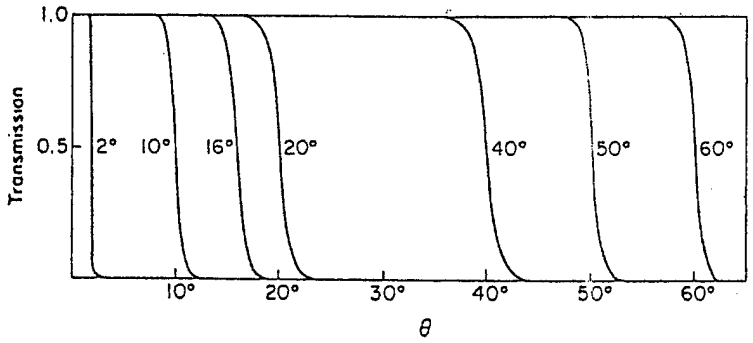

Figure 1-6
Transmission-angle curves for 3-D CPCs with θ_{max} from 2° to 60°.

The light concentration with 2° divergency is close to the smallest achievable with a CPC. However, in this case, the length of the concentrator must be about four meters. Limits of the concentration ratio are established by the Lagrange invariant, which is an interpretation of the energy conservation law in optics. The Lagrange invariant says that the product of the sine of the angular divergency and the beam size of any beam section is a constant, as shown in Figure 1-7.

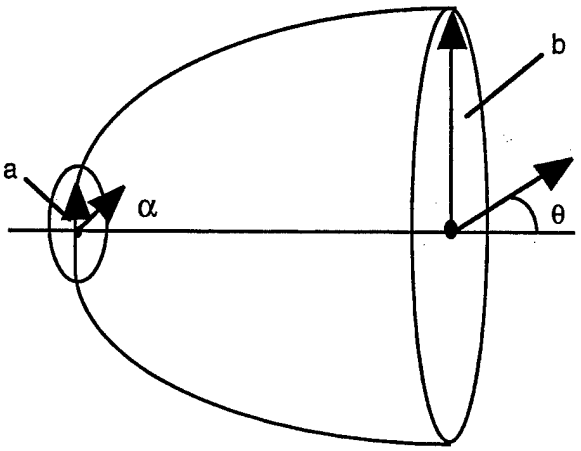

Figure 1-7
Lagrange invariant.

Following the Lagrange invariant:

$$a \sin \alpha \leq b \sin \theta \qquad (1\text{-}1)$$

Equity in Eq. (1-1) is possible only in a perfect design without aberrations. The proposed NIBCC for point sources is an example of the limits of the Lagrange invariant. In this case, the height of the source at the entrance $a = 0$ and $\sin \alpha = 1$, as shown in Figure 1-1. At the exit without aberrations, we will obtain $\sin \theta = 0$. In real life, the image of the fiber end over the GRIN lens cannot be infinitesimal, so a will be greater than 0. Aberrations will appear in the design. In the best case, without aberrations to concentrate light in the angle ±3' for a light source about 0.05 mm and ±80° convergency, using the Lagrange invariant, the NIBCC will have a 57 mm exit diameter. The exit diameter of the prototype of the NIBCC is 85 mm, which is extremely close to the absolute minimum.

1.2.3 Conjugation of NIBCC Surfaces

The nonimaging light concentrator concentrates light from the whole hemisphere. The maximum accepted ray is FA (Figure 1-8). The lateral surface AB is a paraboloid of rotation, which reflects light at the angle of total internal reflection k or at angles greater than this angle.

$$n \sin K = 1, \qquad (1\text{-}2)$$

where n is the refractive coefficient of the nonimaging element material. All rays will be reflected at an angle θ from the optical axis FO (Figure 1-8). After reflection at the conical surface BD, the outgoing rays will be parallel to the axis.

$$n \sin \alpha = \sin \beta \tag{1-3}$$

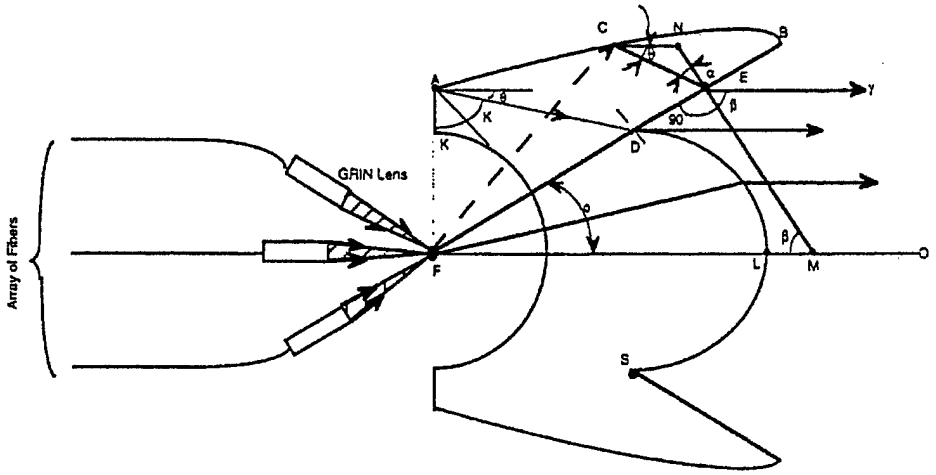

Figure 1-8
Conjugation of the beam-combiner surfaces.

If the outgoing ray γ is parallel to the axis from triangle FEM:

$$\beta = 90° - \phi \tag{1-4}$$

where EM is normal to the conical surface DB. From triangle CNE:

$$\alpha = 180° - \theta - \measuredangle \text{CNE} \tag{1-5}$$

because angle CNE (δ) is

$$\measuredangle \text{CNE} = \delta = 180° - \beta \tag{1-6}$$

or, taking into consideration Eq. (1-4),

$$\delta = 180^\circ - 90^\circ + \phi = 90^\circ + \phi \tag{1-7}$$

so

$$\alpha = 180^\circ - \phi - 90^\circ - \theta = 90^\circ - \theta - \phi \tag{1-8}$$

so the main equation that determines the design of the nonimaging element is the interpretation of Eq. (1-3):

$$n \sin(90^\circ - \theta - \phi) = \sin(90^\circ - \theta), \text{ or}$$

$$n \cos(\theta + \phi) = \cos(\theta). \tag{1-9}$$

Because $\theta = 90^\circ - 2K$, and angle K is known from Eq. (1-2), Eq. (1-9) gives the magnitude of ϕ.

The surface DLS is a convex ellipsoid. The back focus is at point F. It is known that if the eccentricity ε of the ellipsoid is

$$\varepsilon = 1/n \tag{1-10}$$

all rays will exit parallel to the x axis (see Figure 1-9).

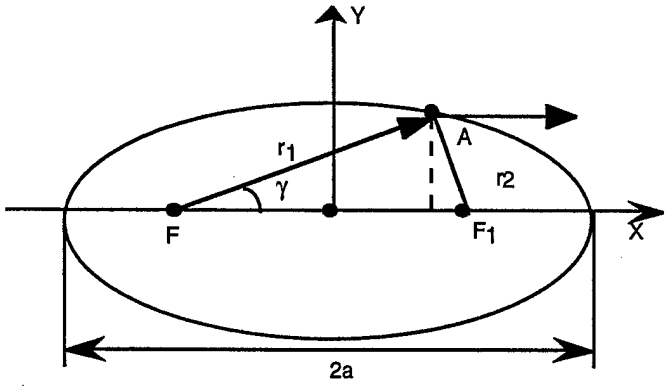

Figure 1-9
Principles of the convex ellipsoid.

If $r_1 = FA$ and $r_2 = AF_1$:

$$r_1 = a + \varepsilon x \tag{1-11}$$

where a is the half axis of the ellipse. If angle γ is equivalent to ϕ, the situation is reflected in Figure 1-10.

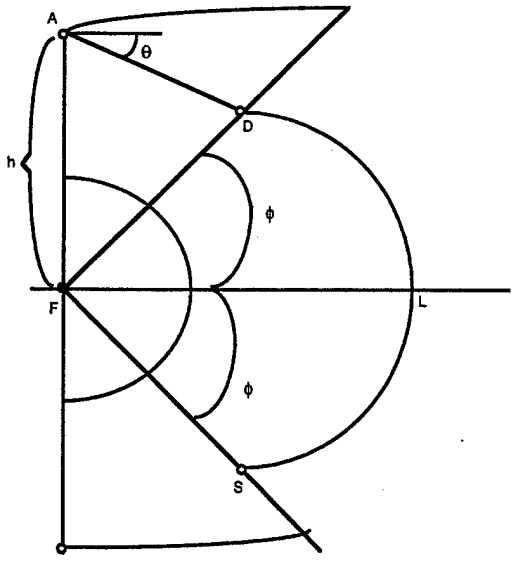

Figure 1-10
Evaluation of ellipsoid parameters.

The segment FD is r_1 for angle ϕ. To find r_1, let's consider the triangle FAD:

$$r_1 / \sin(90-\theta) = h / \sin(180-90+\theta-90+\phi), \tag{1-12}$$

or

$$r_1 / \cos\theta = h / \sin(\theta+\phi)\ , \tag{1-13}$$

$$r_1 = h\cos\theta / \sin(\theta+\phi)\ .$$

Because focal point F is at the position in which x = -aε (Figure 1-9), the x coordinate of point D is:

$$x_D = -a\varepsilon + r_1\cos\phi \tag{1-14}$$

However, from Eq. (1-11), we have:

$$r_1 = a+\varepsilon x_D \text{ or} \tag{1-15}$$

$$r_1 = a+\varepsilon(-a\varepsilon + r_1\cos\phi)\ .$$

Eq. (1-15) will determine parameter a:

$$a = \frac{r_1}{\left(1-\varepsilon^2\right)}(1-\varepsilon\cos\phi) \tag{1-16}$$

Parameter a from Eq. (1-16) and parameter ε from Eq. (1-10) will determine the ellipse. The design shown in Figure 1-8 is theoretically free of aberrations. However, in practice, the light concentrated at point F has a finite size because it is the image of the end fibers over the GRIN lenses. This will lead to divergence of the outgoing beam, which will be discussed in Section 1.2.6.

1.2.4 Evolution of the Shape of the NIBCC with Respect to the Magnitude of the Refractive Index

An NIBCC with an acceptable entrance angle of 180° exists for a very narrow interval of the refractive index of optical material. This interval of the refractive index is limited to index magnitudes from 1.7 to 1.85. Shape degradation of the NIBCC is caused by swelling of the elliptical part of the NIBCC with a decreasing index. This happens because the eccentricity grows with the decreasing index (Eq. (1-10)) and increases the absolute value of the small ellipse axis. This index decrease leads to an increase in the angle of total internal reflection K (Figure 1-8), and hence, in the height of point D. If the index grows, the ellipse shrinks, which will once more lead to shape degradation. Figure 1-11 shows the shape of the NIBCC for different magnitudes of index of refraction.

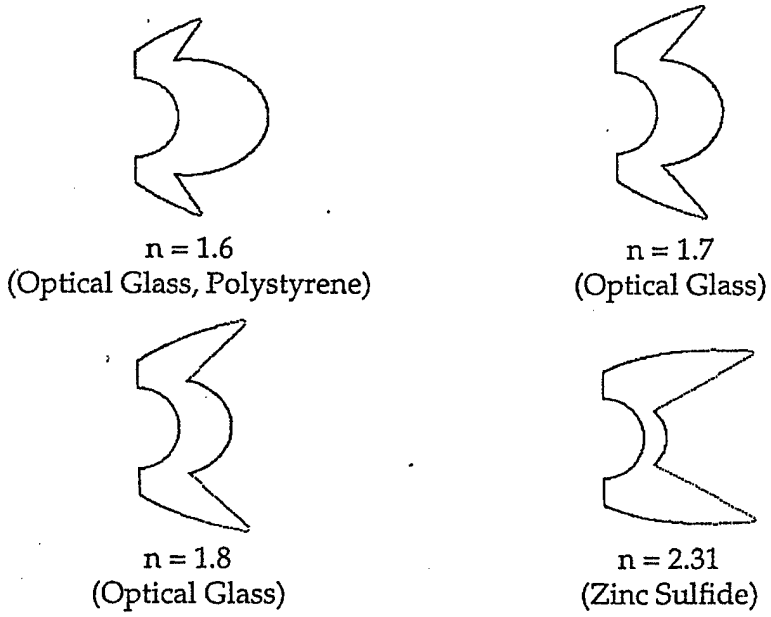

Figure 1-11
Evolution of the shape of the NIBCC with respect to the magnitude of the refractive index.

Diamond turning is the only feasible technology for NIBCC manufacturing. However, using the diamond-turning process with glass creates a ruptured layer. Argus Int. is the only company that

has established the technology of diamond-turning on glass. After performing diamond-turning on glass, this company uses a computer to govern the polishing. Unfortunately, at this time, the company is overloaded with mass production and is unable to manufacture our prototype. Therefore, it was necessary to create a design from optical plastic-acrylic. Acrylic has a refractive index of 1.5, and the only way we could create a realistic design was to reduce the entrance angle from 180° to a lower value. Figure 1-12 shows the conjugation scheme for this case.

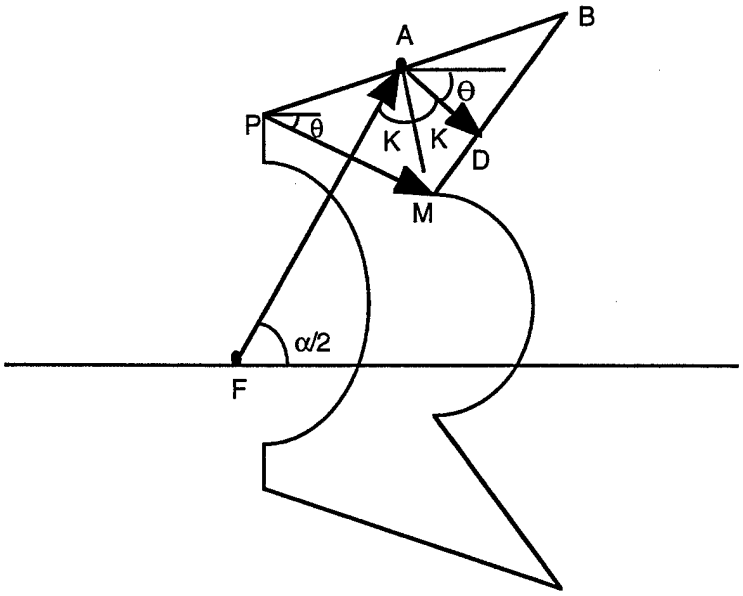

Figure 1-12
Conjugation scheme for the entrance angle α, which is less than 180°.

In Figure 1-12, for the inclined parabola PB, the total internal reflection begins from point A. Despite the large magnitude of angle K, angle θ is sufficiently large to support the compact elliptical part of the NIBCC (ray PM is going down and point M is close to F). In this case, the ellipse does not swell. In Figure 1-1, $\theta = 902K$. Now $\theta = 90-2K+(90-\alpha/2)$. The segment DM is not functional in this design, because of the leakage of light over the parabola segment PA. The elliptical part is the main source of aberration in the NIBCC, even though it is sufficiently small in this design. Therefore, the fiber optic illumination assembly must be in accordance with the acceptance angle of the NIBCC.

1.2.5 Ray Tracing Over an Arbitrary Optical Surface

Ray tracing is the main computer instrument for estimating image quality and providing system optimization. Conventional optical surfaces such as spheres can be described in a Cartesian coordinate system with a second order equation. To find the point at which the arbitrary ray intersects with this surface, a quadratic equation must be solved. The procedure of ray tracing over second order surfaces was investigated thoroughly and named the Feder method [9]. The NIBCC consists of several surfaces. One of them is an inclined parabola, which is a high order surface. For ray tracing over such a surface, only a common method of nonlinear equation solution can be applied. Figure 1-13 depicts the problem of finding the arbitrary ray's point of intersection with the direct vector $\bar{r}$ from point A with the arbitrary surface $F(x,y,z)=0$.

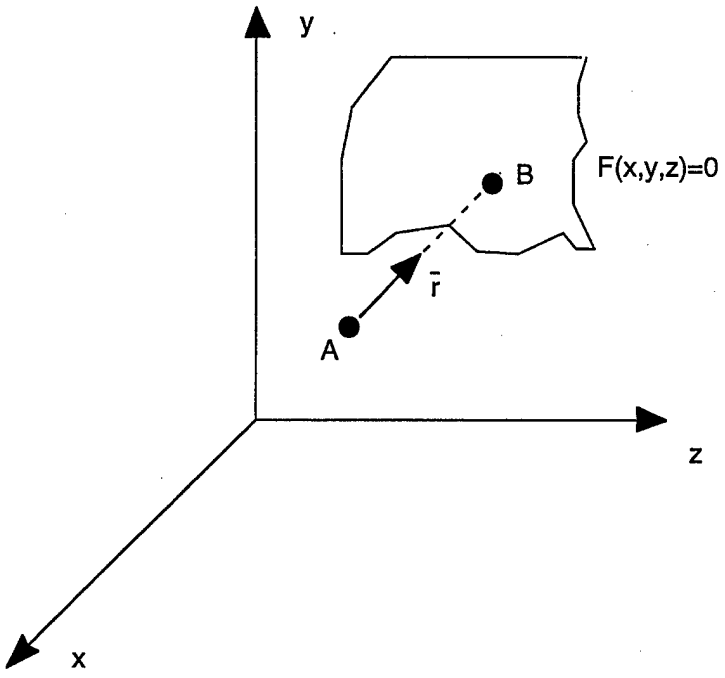

Figure 1-13
Coordinates of ray-surface intersection determination.

To find the point of intersection, it is necessary to solve the nonlinear equation system in which the first is a surface equation and the second is a ray equation.

$$\begin{cases} F(x,y,z)=0 \\ \bar{a}+\bar{r}\Delta\ell=0 \end{cases}, \tag{1-17}$$

where $\bar{a}$ is the vector coordinate at point A and $\Delta\ell$ is the arbitrary distance shift along the ray from point A. We can rewrite it as:

$$F(\bar{a}+\bar{r}\Delta\ell)=0 \tag{1-18}$$

To solve Eq. (1-18), the Newton method can be used. Eq. (1-18) can be solved in the first approach as:

$$F(x_A,y_A,z_A)+F_x'\Delta x+F_y'\Delta y+F_z'\Delta z=0, \tag{1-19}$$

or

$$F(x_A,y_A,z_A)+\left(F_x'rx+F_y'ry+F_z'rz\right)\Delta\ell=0 \tag{1-20}$$

and

$$\Delta\ell=-F(x_A,y_A,z_A)\Big/\left(F_x'rx+F_y'ry+F_z'rz\right), \tag{1-21}$$

where rx, ry, rz, are the direction cosines of the vector $\bar{r}$.

After $\Delta\ell$ is found, the new coordinate of point A is calculated (vector coordinate a'):

$$\bar{a}'=\bar{a}+\bar{r}\Delta\ell \tag{1-22}$$

The process continues from the new approach point, and iterations are conducted until $\Delta\ell$ has a significant value.

Ray tracing is conducted over all the surfaces, from the image of the fiber tip to the illuminated plane. Refraction and reflection are described by Snell's law [9]. The rays are arranged in beams that originate from a number of points on the image of the fiber and at the focal point of the NIBCC. The numerical apertures of the ray bundles are in accordance with the product of the numerical aperture of the delivery fiber and the magnification (V) of the GRIN lens. The ray

tracing ends at the illuminated plane. All rays are considered to have equal energy. The maximum deviation r_{max} of rays from the center of the illumination plane is determined, the illuminated plane is divided into a number of square patches, and the number of rays delivered to every patch is calculated. In the results (which will be shown in next section), the illuminated plane was divided into 9×9 patches. The number of rays reaching every patch is calculated, and the energy at every patch is summarized. Then energy at all the patches is normalized to the maximum. The results are shown on the computer screen in the window entitled "Light spot illumination." To combine the illumination from all the fibers, the software is arranged like a multidocument interface. The special program recalculates all the single fiber intensities to a maximum intensity among all the fibers and summarizes it. The sizes of all the light spots in this software are preserved as the size of the first fiber spot for multifiber calculations. The fiber tip image can be inclined, as shown in Figure 1-14.

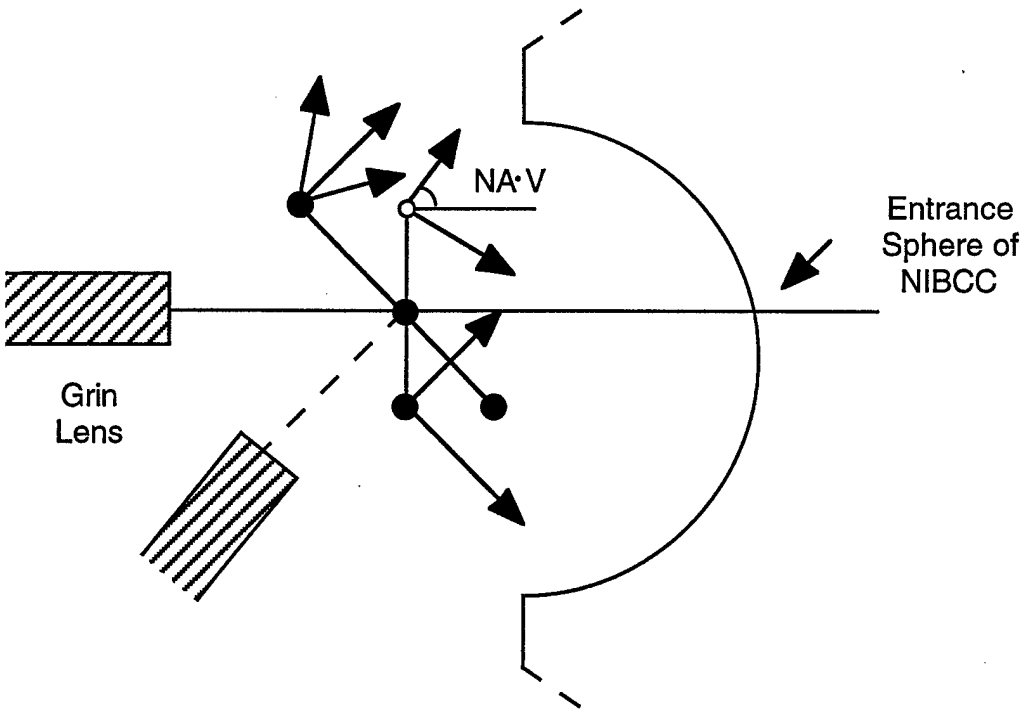

Figure 1-14
Consideration of a light source for the NIBCC in the simulation software.

In this step, the image of the fiber tip was considered to be without aberrations, and the NIBCC and the fiber delivery assembly were optimized separately.

1.2.6 NIBCC Optimization

Due to reasons outside POC's control, the NIBCC could not be manufactured from glass at this time (see Section 1.2.4). Therefore, the NIBCC was produced from optical acrylic. It was ordered from the Lumonics Optics Group in Canada, where it was manufactured by using diamond-turning technology. The simulation software demonstrates that the optimal entrance angle, which is independent from the fiber tip image diameter, is 160°. In other initial data for optimization, the diameter of the image of the fiber tip is 0.05 mm, and the numerical aperture (NA) of the incoming beam is 0.37 (± 22°). These data are accepted at this stage of modeling because of the limited choice of the GRIN lens. A trade-off between the size of the image of the fiber tip and the filling the entrance aperture will be considered in the next section. The result of optimization is shown in Figures 1-15 and 1-16. Figure 1-15 shows the computer simulation of the axial beam. In Figure 1-16, the beam is inclined at 60°.

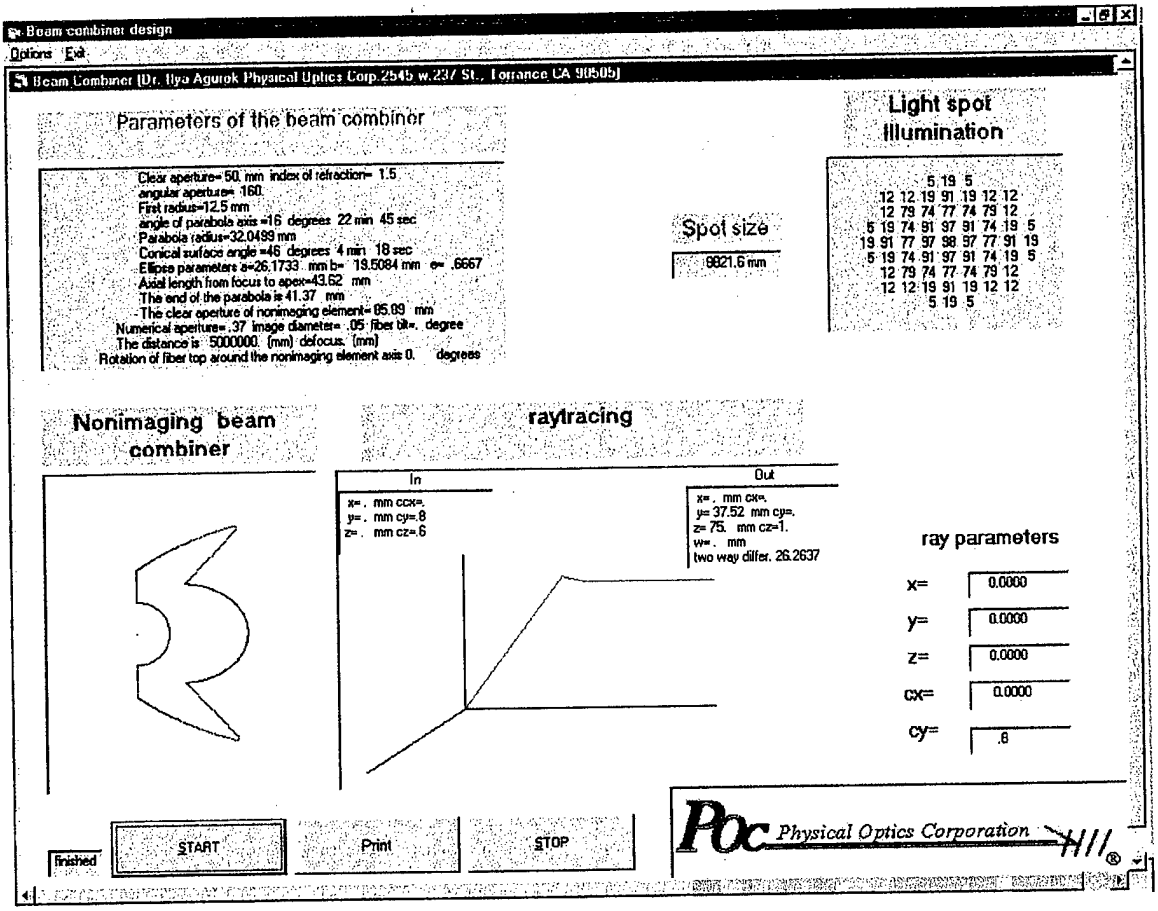

Figure 1-15
Axial beam illumination simulation.

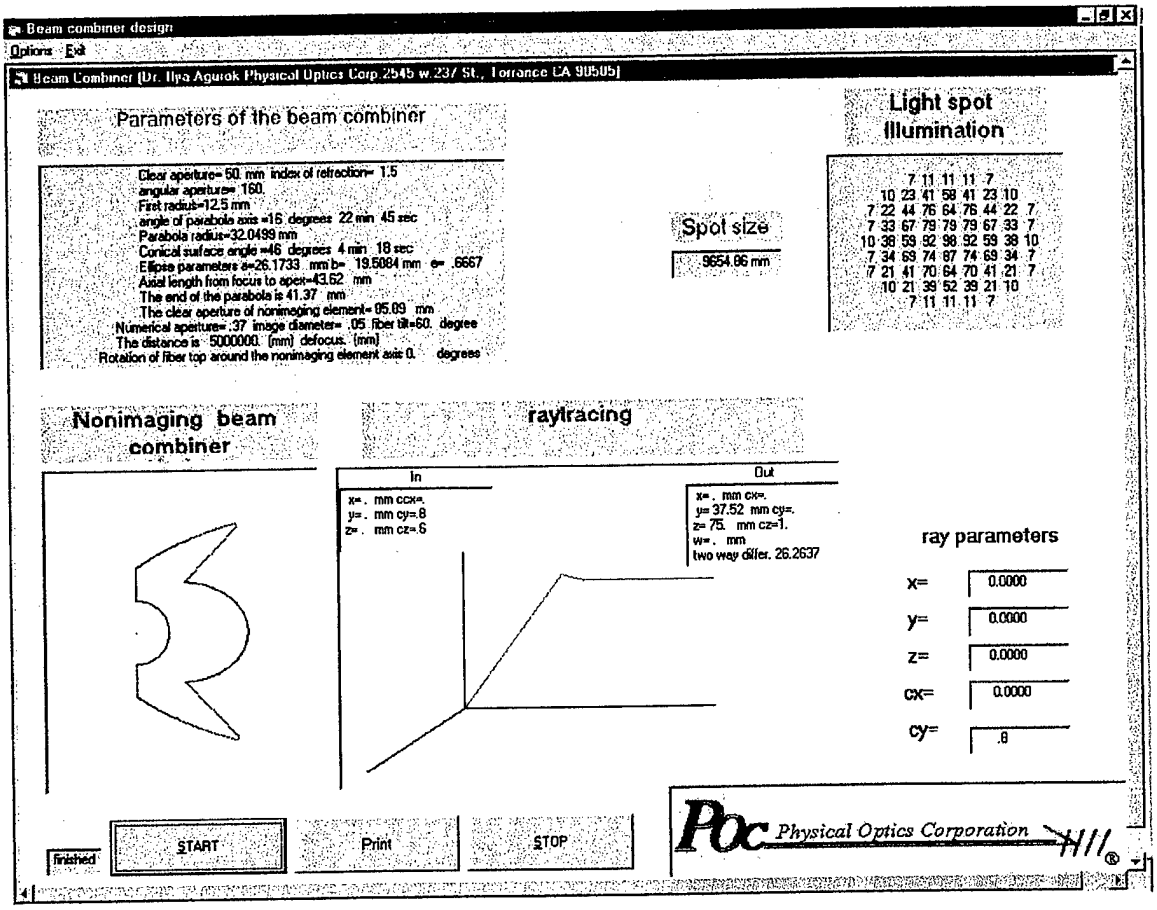

Figure 1-16
60° entrance beam simulation.

The light spot in Figure 1-16 is 9654 mm in size at a 5 km distance from the NIBCC. The light spot for the axial beam (Figure 1-15) is 8821 mm. This means that we have achieved beam divergence of about $\pm 3.2'$. The length of the NIBCC is 43.62 mm. The output diameter is 85.9 mm. The detailed parameters of the element are shown in the tables on the upper left in Figures 1-15 and 1-16. In the right-hand table, under the title "Light spot illumination," the light intensity distribution is shown. The distribution for the axial beam is very close to a rectangular shape. The distribution for the off axial beam gives something close to a Gaussian fourth order function. Potentially, this design can combine the light from seven laser diodes, as shown in Figure 1-17. This scheme provides a 164° entrance angle for the NIBCC (Figure 1-18).

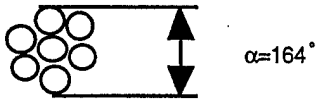

Figure 1-17
Combination of seven beams by the NIBCC.

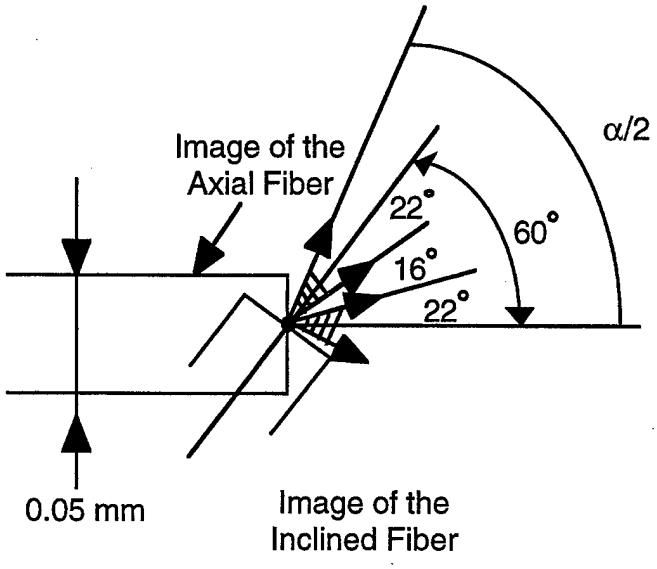

Figure 1-18
Interaction of the input beams.

A three-dimensional scheme was chosen for device prototyping. In this scheme, the light from three diodes combines into one beam. The input beams are evenly spaced. The angles between input beams are 60°. The angle between the axis and the GRIN lens axes is 45° (Figure 1-19).

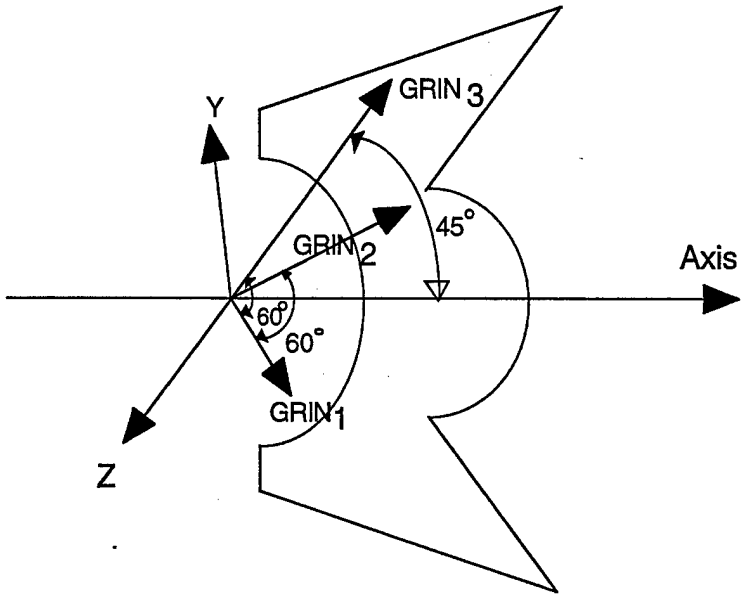

Figure 1-19
Beam combination in one plane.

1.2.7 Fiber Optics Delivery Assembly

The light source for the prototype was chosen. We purchased 0.635 μm wavelength light emitting diodes from LaserLyte Corp. The laser diodes are coupled into a multimode fiber with a core ϕ 0.062 mm, NA = 0.37. To focus this light, a cylindrical Selfoc SLM series 1.8 mm diameter GRIN lens was chosen. This GRIN lens is shown in Figure 1-20.

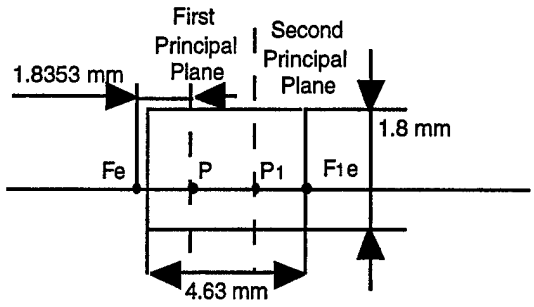

Figure 1-20
Selfoc GRIN lens.

GRIN lenses have a common problem: the aperture stop is inside the lens. Therefore, the mechanical diameter of the GRIN lens is greater than the clear aperture. This is shown in Figure 1-21 [14].

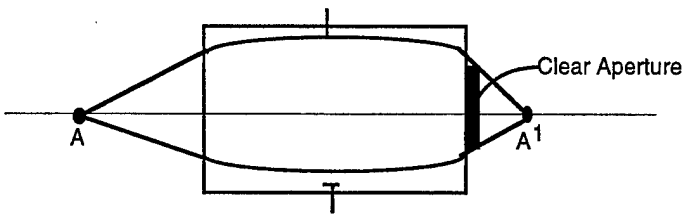

Figure 1-21
Aperture stop inside the lens.

This will prevent complete filling of the input cone for the NIBCC shown in Figure 1-17. This situation is reflected in Figure 1-22.

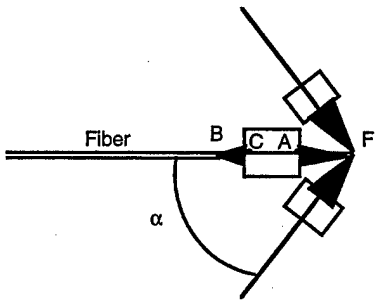

Figure 1-22
Incomplete filling of the input cone for the NIBCC.

To achieve angle $\alpha = 60°$, segment AF must be 1.55 mm long. Hence, BC = 2.1728 mm.

$$BC = f_{lens}^2/1.55 = 1.6352^2/1.55 = 2.1728 \text{ mm} \qquad (1\text{-}23)$$

In this case, if the clear aperture is approximately 1.4 mm (Figure 1-21) of the mechanical lens diameter, the entrance GRIN lens aperture is 0.28 instead of the exit fiber aperture of 0.37. Thus, we will lose some amount of light. The magnification is 0.84 and the image of the fiber tip

diameter is 0.050 mm. The problems of not filling the GRIN lens aperture and the incomplete filling of the input cone will be considered in Phase II. To increase the outgoing aperture of the fiber delivery assembly, a diffuser was placed at the point F in Figure 1-22. The assembly of the GRIN lens and the delivery fiber is shown in Figure 1-23.

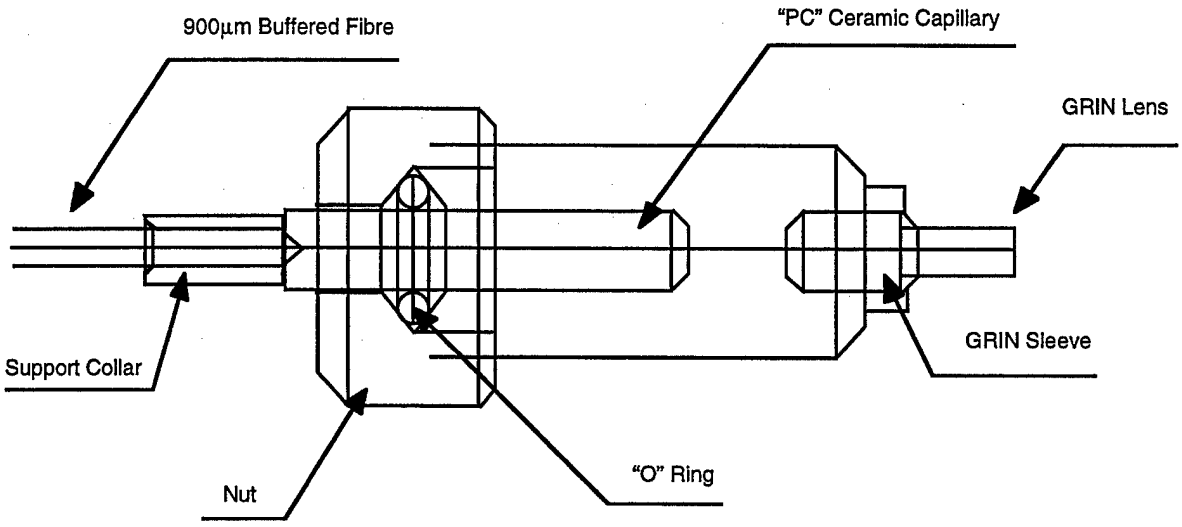

Figure 1-23
Assembly of the delivery fiber and the GRIN lens.

The nut makes it possible to axially align the ceramic capillary with respect to the GRIN lens. All other alignment shifts can be achieved by mechanical assembly of the prototype, described in Section 1.2.8.

1.2.8 Mechanical Assembly of the NIBCC Prototype

The mechanical assembly of the NIBCC prototype is shown in Figure 1-24.

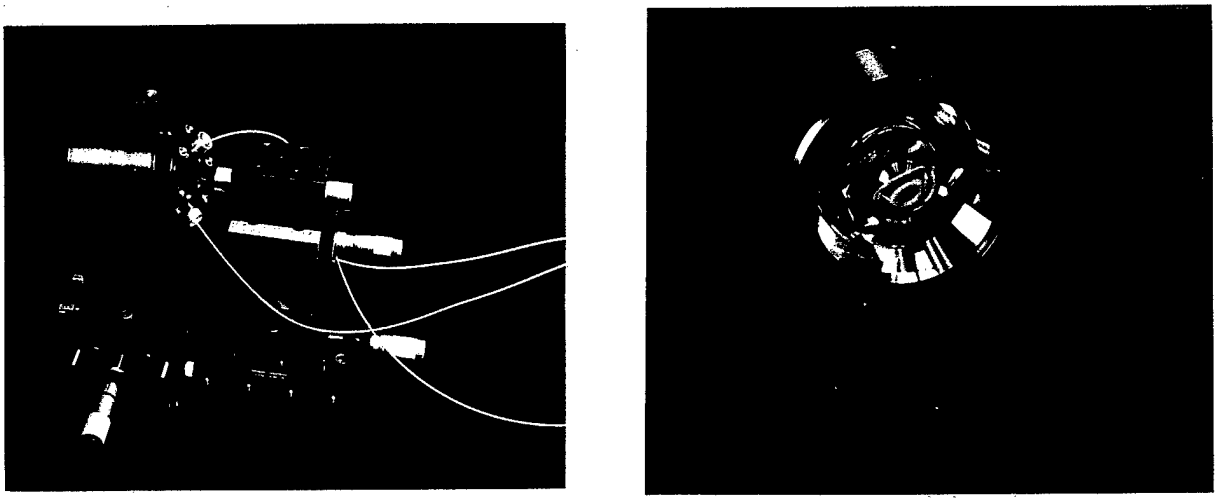

(a) Mechanics. (b) Beam combiner in housing.

Figure 1-24
Mechanical assembly of the NIBCC prototype.

The mechanical assembly consists of two main parts. The first (1) is the beam combiner housing. It is mounted on the rotation stage with one precise lateral movement. The fiber-GRIN lens assembly (2) is mounted on the precise three-dimensional movement stage. The fiber-GRIN lens assembly has three-dimensional alignment screws for focusing light in one spot. To achieve focusing, the pinhole is mounted to the top side of the assembly and all three of the GRIN lenses are focused in one point. Then the pinhole is removed and replaced by the diffuser, which provides smooth illumination inside the aperture. The housing of the beam combiner conforms with the shape of the beam combiner, which leads to some dispersed light in the image plane. This is shown in Figure 1-25.

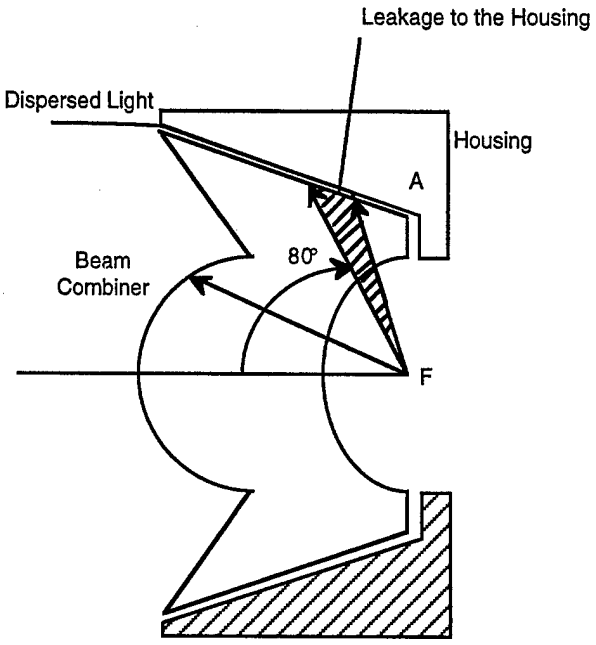

Figure 1-25
Dispersed light from the housing.

As shown in Figure 1-12, the beam combiner was designed for a ±80° entrance aperture. If some light enters the beam combiner at a greater angle, it will leak into the housing surface and be reflected by it, as at point A in Figure 1-25. In our future design, this part of the housing surface will include a light absorption buffer.

1.2.9 Beam Performance in the Prototype

The beam performance in the near vicinity of the beam combiner is shown in Figure 1-26.

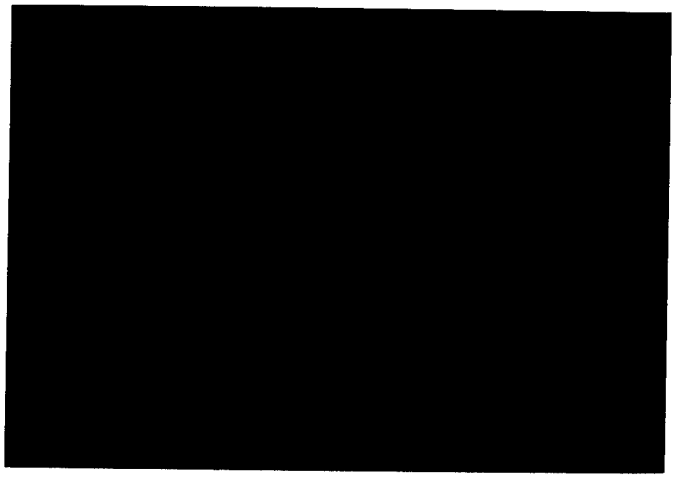

Figure 1-26
Near vicinity of the beam combiner.

Two zones of illumination can be distinguished. The central zone is an elliptical zone. The lateral light goes to the inclined parabola and is reflected and refracted at the conical surface. There is no total internal reflection over zone AB in Figure 1-27.

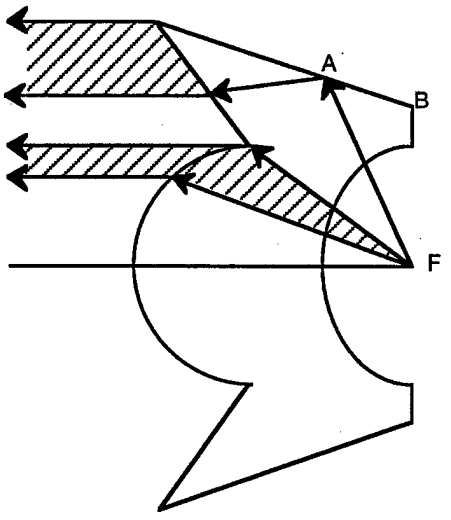

Figure 1-27
Interaction of the outgoing light in the vicinity near the combiner.

Then, at a distance of 9 meters, these three beams recombine into three light spots with an overall pictured diameter of 115 mm (Figure 1-28). Because the diameter of the beam combiner was 85 mm originally, this means that the divergence of the outgoing beam is ±5.5'.

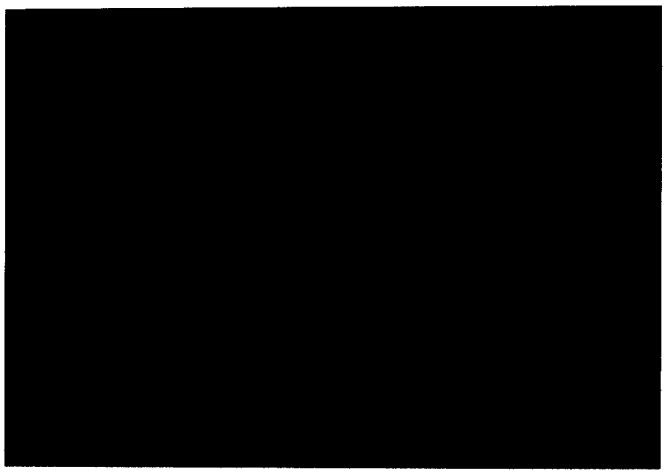

Figure 1-28
Light spot at a distance of 9 m.

In the case of seven fibers, the light emission will be assembled in one spot, so we will have an evenly illuminated spot.

1.2.10 Improvement in Focusing Optics

The image quality of the focusing optics (as shown in Figure 1-23), with a single plano-plano GRIN lens, is far from the condition in which the assembly with a beam combiner can achieve a beam divergence of $\pm 3'$. The main problem of this schematic is the aberrations, which increase the light spot size of the focal plane of the beam combiner from 0.05 mm to 0.5 mm. The new scheme was developed with a plano-convex GRIN lens [14] and an additional positive component. The additional positive component compensates for aberrations and makes the input aperture equal to the fiber aperture, 0.35. The scheme is shown in Figure 1-29.

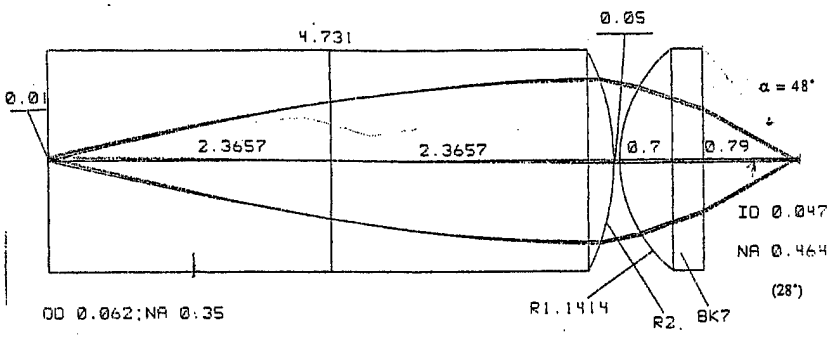

Figure 1-29
Focusing scheme with Selfoc microlens PCW 180 025 083 with a positive component.

This scheme, which is shown in Figure 1-30, provides good aberration correction. In Figure 1-30, the three point spread function for object heights 0, 0.02 mm, and 0.031 mm are shown.

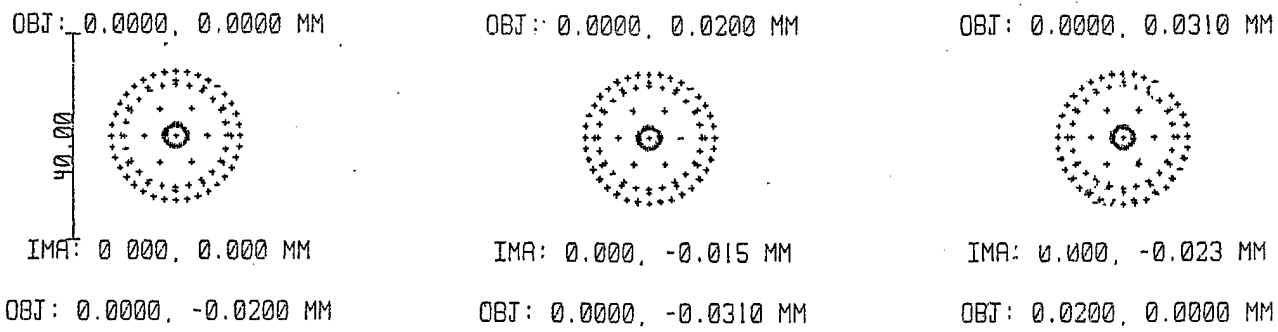

Figure 1-30
Image quality for the focusing scheme.

The spot size is about 0.015 mm in diameter. This means that the image of the fiber tip over the focusing system will appear as shown in Figure 1-31.

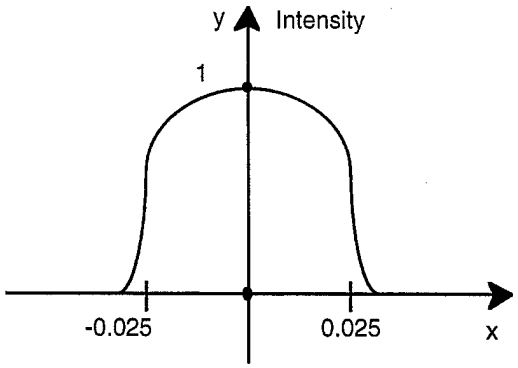

Figure 1-31
Image of the fiber tip.

However, one problem still persists in this schematic. The beams cannot be mechanically combined into one continuous beam. The outgoing aperture of the scheme is 0.464 (±28°), but the mechanically assigned aperture is ±48°. With this aperture, the positive lenses can be combined edge to edge. To project the exit pupil over the positive lens, a negative lens must be added to the scheme. This is shown in Figure 1-32.

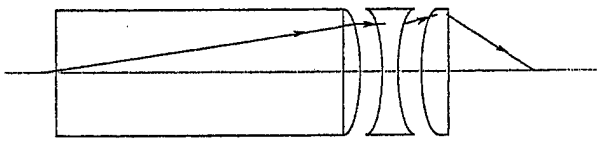

Figure 1-32
Improved scheme for comprehensive beam combining.

This scheme was developed and is shown in Figure 1-33.

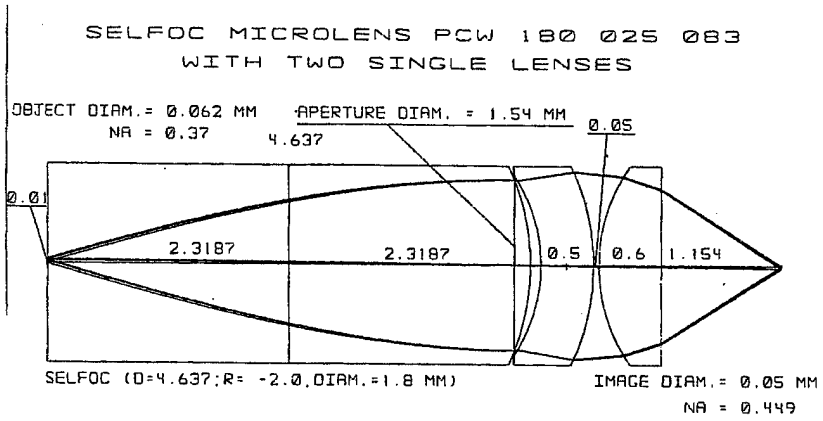

SELFOC (D=4.637; R=-2.0; DIAM.=1.8 mm)			IMAGE DIAM. =0.05 mm	
R1=-1.408	D1=0.10			NA=0.449
R2=-1.971	D2=0.50	TF10	Diam. 1.8 mm	n_{TF10} =1.7999
R3=1.499	D3=0.05	CTK19	Diam. 1.8 mm	n_{CTK19} =1.7410
R4=0	D4=0.60			

Figure 1-33
High quality focusing objective.

The image quality of this objective is 10 times better than for the objective in Figure 1-29. The maximum spot size at the edge of the field-of-view is about 2 μm. The point spread functions of this objective for four field-of-view points are shown in Figure 1-34.

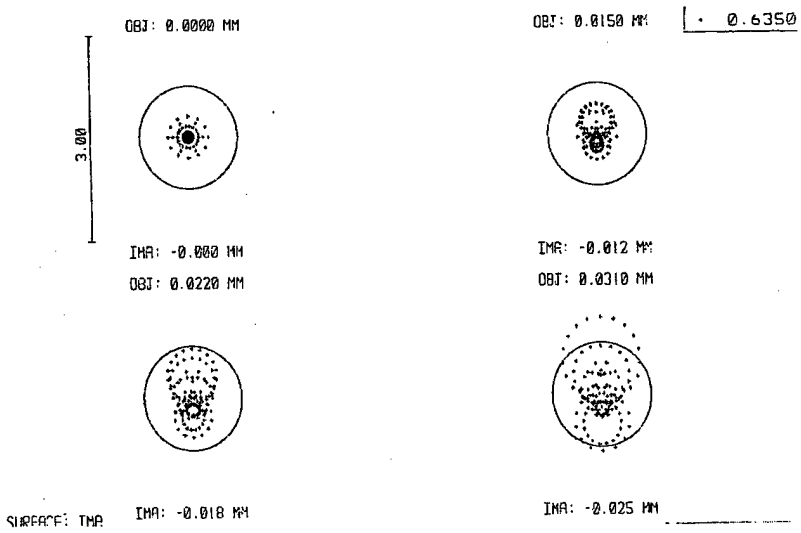

Figure 1-34
Image quality for the three-component focusing systems.

The exit aperture of the developed focusing objective is 0.449, or 26°. So the double angle of the light cone is 52°. The arrangement of the seven objectives, which is shown in Figure 1-17, can cover the entrance cone of the NIBCC, 156°. The optics of the objective have to be assembled into a mechanical housing. The minimum thickness of the housing walls is 0.2 mm. This is the reason that the entrance aperture of the NIBCC cannot be completely filled. With an image distance of 1.154 mm, shown in Figure 1-33, the minimum half angle of beam interruption is about 9°. A possible housing design of the focusing objective is shown in Figure 1-35.

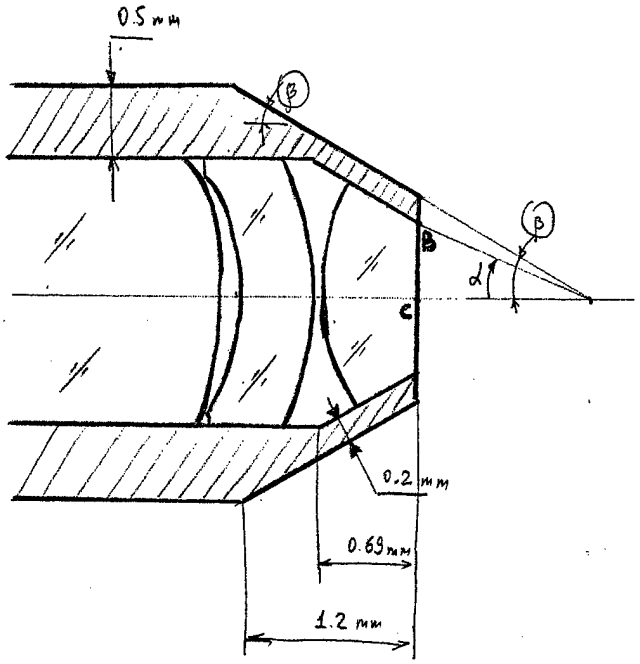

$\alpha = 23°$
$\beta = 30.8°$
BC = 0.49 mm

Figure 1-35
Possible mechanical housing for the focusing objective.

The possible arrangement of beams incident on the NIBCC with this objective is shown in Figure 1-36.

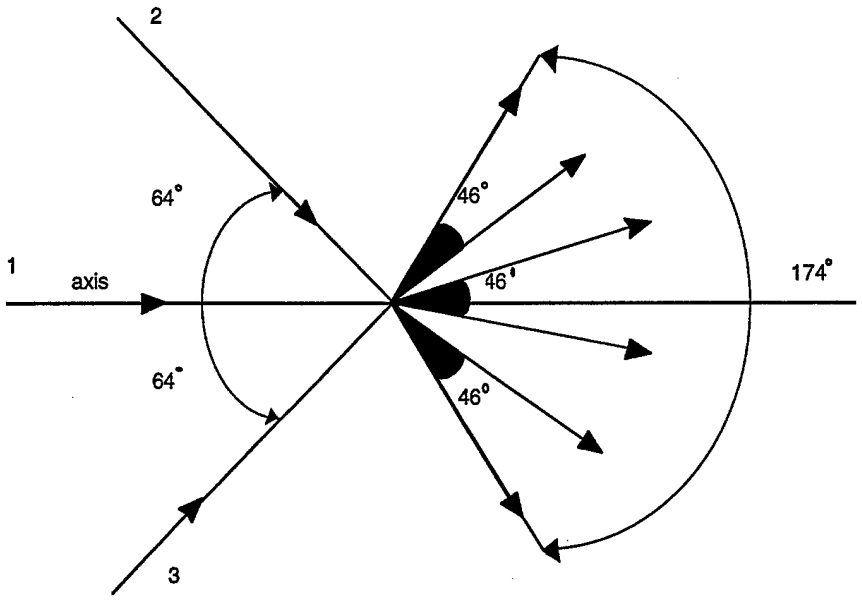

Figure 1-36
The arrangement of incident beams on the NIBCC.

The arrangement in Figure 1-36 is close to optimal and can be achieved with existing micro-objective manufacturing technology.

1.2.11 Problem of Light Dispersed at the Elliptical Surface

The investigation of the NIBCC prototype revealed that part of the elliptical surface receives light at the incident angles, which are close to the total internal reflection angle. This is shown in Figure 1-37.

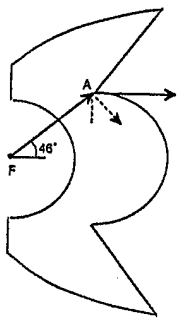

Figure 1-37
Problem with total internal reflection at the elliptical surface.

The incident angle at point A in Figure 1-37 is close to the total internal reflection (TIR) angle. At this angle, the reflection component of the incident light begins to overcome the refraction mode. This is shown in Figure 1-38.

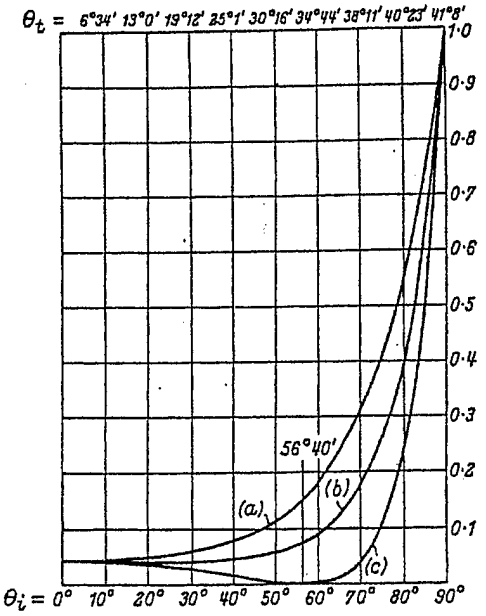

Figure 1-38
Intensity of reflected light as a function of the angle of incidence.

To overcome this problem, the input beams can be arranged as shown in Figure 1-39. In Figure 1-39, the central input beam has a ±46° aperture and 40° peripheral beams.

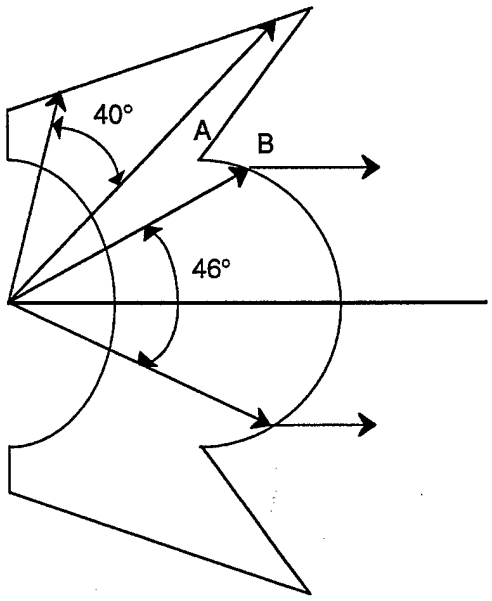

Figure 1-39
The way to avoid the TIR condition at the elliptical surface.

1.2.12 Commercial Applications of the Proposed Technology

The main advanced feature of the proposed NIBCC is its ability to combine light from several laser diodes into an extremely collimated beam. For this reason, we can achieve a bright, well focused beam, which can be achieved only with incandescent light sources that are 10 times more powerful. The small dimensions of the NIBCC constitute another advanced feature that is very attractive for commercial applications. Thus, it can be utilized in airport landing light devices, high mast warning lights, navigation lights, portable police searchlights, and laser diode target designators.

2.0 CONCLUSION

During Phase I, POC developed a prototype of the NIBCC which demonstrated very advanced optical characteristics. The divergence of the outgoing beam is only ±5.5'. This is larger than the required ±3', but can be improved with subsequent NIBCC development in Phase II. The ways to improve the prototype were discussed in Sections 1.2.8 to 1.2.11 of this report. Investigation

of the prototype demonstrated that the innovative NIBCC is a feasible device from the perspective of optical technology and offers a promising commercial outlook.

3.0 REFERENCES

1. B. Stann, W. Ruff, and Z. Sztankay, "Intensity-modulated diode laser radar using frequency-modulation/continuous-wave ranging techniques", *Optical Engineering* 35(11), 3270-3278 (1996).
2. C. Garvin, C. Deluca, G. Sztankay, B. Stann, et al., "Multi-domain smart sensor testbed field operation at FT AP HILL," *3rd Annual Fed Lab. Symposium,* pp. 15-21 (Feb. 2-4, 1999).
3. "Nonimaging Beam Combiner-Collimator," POC proposal #98-312 AT.
4. W.T. Wilford and R. Winston, "High Collection Nonimaging Optics," *Academic Press* (1981).
5. J. Spiguls, "Compact dielectric refractive element," *Appl. Opt.*, vol. 33, no. 25, pp. 5970-5974.
6. J. Flores, "Geometrical optics of gradient index lenses," *Optical Engineering*, vol. 28, no. 11, pp. 1173-79.
7. Dr. Luke Lester, University of New Mexico (private conversation).
8. Power Technology Inc. product catalog (1998).
9. M. Born and E. Wolf, *Principles of Optics*, Pergammon Press (1982).
10. I. Agurok and A. Rizkin, "Nonimaging beam transformer design and optimization for marine navigation light," *SPIE 42nd Annual Meeting*.
11. R. Winston, "Light collection within the framework of geometrical optics," *J. Opt Soc. Am.*, 60, 245-247 (1970).
12. I. Agurok and A. Rizkin, "Light transformer design and optimization," *OSA, Annual Meeting* (1995).
13. R. Winston, "Dielectric compound parabolic concentrators," *Appl. Opt.*, 15, 291-292, (1970).
14. Selfoc catalog.